Prediction of the Impact Point for Spin and Fin Stabilized Projectiles

DIMITRIOS N. GKRITZAPIS
Hellenic Army Academy
Vari, 16673, Athens
GREECE
gritzap@yahoo.gr

DIONISSIOS P. MARGARIS
Mechanical Engineering and Aeronautics Dept.
Fluid Mechanics Laboratory, University of Patras, 26500 Patras
GREECE
margaris@mech.upatras.gr

ELIAS E. PANAGIOTOPOULOS
Mechanical Engineering and Aeronautics Dept.
Fluid Mechanics Laboratory, University of Patras, 26500 Patras
GREECE
hpanagio@mech.upatras.gr

GEORGE KAIMAKAMIS
Hellenic Army Academy
Vari, 16673, Athens
GREECE
gmiamis@gmail.com

KONSTANTINOS SIASSIAKOS
Hellenic Naval Academy
Piraeus, 18539
GREECE
siassiakos_k@ideke.edu.gr

Abstract. A method for real time in flight prediction of the ground impact point of indirect fire projectiles is investigated. The projectiles is assumed to be both rigid (non-flexible), and rotationally symmetric about its spin axis launched at low and high pitch angles. A six degree of freedom projectile model solution is used to propagate the projectile state from an arbitrary point along the trajectory to the ground impact point. The projectiles manoeuvring motion depends on the most significant force and moment variations, in addition to gravity. The developed computational method gives satisfactory agreement with published data of verified experiments and computational codes on atmospheric projectile trajectory analysis for various initial firing flight conditions.

Keywords—Aerodynamic forces and moments, low and high pitch angles

1 Introduction

Exterior ballistics existed for centuries as an art before its first beginnings as a science. Although a number of sixteenth and seventeenth century European investigators contributed to the growing body of renaissance knowledge, Isaac Newton of England (1642-1727) was probably the greatest of the modern founders of exterior ballistics. Newton's laws of motion established, without which ballistics could not have advanced from an art to a science. Benjamin Robins of England (1707-1751) developed the first successful ballistic pendulum in 1740, based on an idea proposed by the younger Cassini in 1707. Charles Hutton (1737-1823), who succeeded Robins at Woolwich, obtained drag results for spheres between 1787 and 1791 that showed close agreement with Robins' measurements.
In 1851, Captain Minié of France invented the "Minié Ball", an ogival-cylindrical bullet with a conical base cavity to provide obturation in a rifle barrel. After about

1850, ballisticians of many countries began experiments to improve the accuracy of drag measurements. Francis Bashforth of England invented the Bashforth electro-chronograph, based on circuitry developed by Charles Wheatstone, inventor of the Wheatstone bridge. From 1875 to 1881, the Krupp factory at Meppen Proving Ground, Germany, conducted a large number of air resistance firings, using three different projectile shapes.
In 1883, General Mayevski analyzed the Krupp firing data and formulated his "zone" laws of air resistance for a projectile about three calibers long, having a flat base and an ogival head with a two-caliber radius. Colonel James M. Ingalls of the U.S. Artillery converted Mayevski's results into English units, and based his tables on them. Ingall's Tables were first published as Artillery Circular M, in 1900. From 1873 to 1898, the Gârve Commission of the French Naval Artillery conducted numerous air resistance firings at the Gârve Proving Ground, utilizing the Boulengé chronograph, which had been developed in Belgium around 1864.
During the first decade of the century, the German firm of Krupp investigated the effect of long slender ogives on the drag of small caliber projectiles. In addition, at the First World War, the Krupp firm used the ten-caliber radius ogive design for 210 mm Paris Gun projectile, which was used to bombard Paris from 120 kilometers range. By the end of the First World War, ballisticians of many countries had recognized the fact that the longer ogives and boattails of the projectiles then in current use were not accurately represented. From 1922 to 1925, R. H. Kent and H. P. Hitchcock of the Ballistics Section, Aberdeen Proving Ground, Maryland, conducted resistance firings of a 3.3-inch shell called "Type J". Moreover, from about 1925 until the end of the Second World War, they conducted numerous yaw card firings, at the same Ballistics Section. On the battlefield, it is well known that the target effects using artillery systems diminish exponentially with the number of rounds fired at a particular target. To maximize target effects, rounds must be designed to hit a target with a minimum number of rounds that impact the target in rapid succession [18], [19]. The modern science of the exterior ballistics [15] has evolved as a specialized branch of the dynamics of rigid bodies, moving under the influence of gravitational and aerodynamic forces and moments.

Pioneering English ballisticians Fowler, Gallop, Lock and Richmond [11] constructed the first rigid six-degree-of-freedom projectile exterior ballistic model. Various authors has extended this projectile model for lateral force impulses [5]-[13], linear theory in atmospheric flight for dual-spin projectiles [3]-[9], aerodynamic jump extending analysis due to lateral impulsives [7] and aerodynamic asymmetry [6], instability of controlled projectiles in ascending or descending flight [14]. Costello's modified linear theory [14] has also applied recently for rapid trajectory projectile prediction. Exterior ballistics encompasses the period from when the projectile has left the muzzle until impact with the target. In general, all that the exterior ballistician is required to know is the muzzle velocity and tip-off and spin rates from the interior ballistician, and the physical properties (shape and mass distribution) from the projectile designer. In exterior ballistics, one generally is concerned with projectiles dynamics and stability, the predicted flight path and time of flight, and angle, velocity and location of impact. The modern science of exterior ballistics has evolved as a specialized branch of the dynamics of rigid bodies, moving under the influence of gravitational and aerodynamic forces and moments [2], [4], [6], [16] [17].

The present work address a full six degrees of freedom (6-DOF) projectile flight dynamics analysis for accurate prediction of short and long range trajectories of high spin and fin-stabilized projectiles. The proposed flight dynamic model takes into consideration the influence of the most significant force and moment variations, in addition to gravity.

The efficiency of the developed method gives satisfactory results compared with published data of verified experiments and computational codes on dynamics model analysis of short and long-range trajectories of spin and fin-stabilized projectiles.

2 Projectile Model

The present analysis considers two different types of representative projectiles. A projectile of 40mm grenade, M781 is presented in Fig. 1, and is used with M203 grenade launcher. The M203 grenade launcher is a lightweight, single-shot, breech-loaded, pump action (sliding barrel), shoulder-fired weapon that is attached to an M16 rifle series. The projectile contains an orange powdered dye which is dispersed on impact. The projectile is blue plastic with white markings. The 120 mm (Fig. 2) Mortar System provides an organic indirect-fire support capability to the manoeuvre unit commander. It is a conventional smoothbore, muzzle-loaded mortar system that provides increased range, lethality and safety compared to the World War II-vintage 4.2-inch heavy mortar system it replaces in mechanized infantry, motorized, armored and cavalry units. A complete family of 120 mm Enhanced Mortar Ammunition is being produced by several government and commercial sources. The M933/934 high explosive round also received full materiel release and is in production. The M929 white phosphorus/smoke received full materiel release in the second quarter of 1999 and is in production. Basic physical and geometrical characteristics data of the above-mentioned 105 mm HE M1 projectile and the non-rolling, finned 120 mm HE mortar projectile illustrated briefly in Table 1.

Fig. 1. 40 mm grenade, M781, launcher ammunition

Fig. 2. The non-rolling finned 120 mm HE mortar projectile

Characteristics	120 mm HE mortar projectile	40 mm grenade, M781
Reference diameter, mm	119.56	40
Total length, mm	704.98	102.9
Weight, kg	13.585	0.205
Axial moment of inertia, kg·m^2	$2.335 \cdot 10^{-2}$	$3.863 \cdot 10^{-5}$
Transverse moment of inertia, kg·m^2	$2.3187 \cdot 10^{-1}$	$3.687 \cdot 10^{-5}$

Table 1. Physical and geometrical data of 40 mm and 120mm projectiles types.

3 Physic Mathematical Trajectory Model

A six degree of freedom rigid-projectile model [1], [8], [10], [12] has been employed in order to predict the "free" nominal atmospheric trajectory to final target area without any control practices. The six degrees of freedom flight analysis comprise the three translation components (x, y, z) describing the position of the projectile's center of mass and three Euler angles (φ, θ, ψ) describing the orientation of the projectile body with respect to Fig. 3.

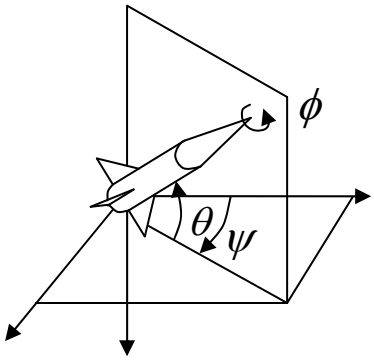

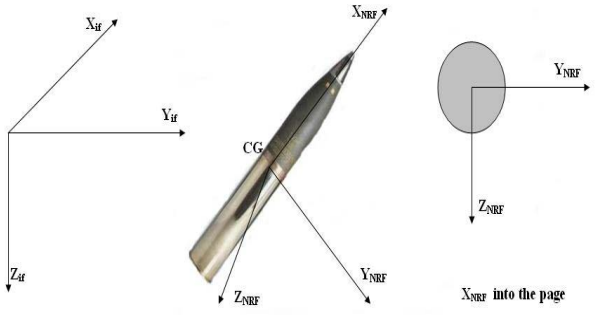

Fig. 3. No-roll (moving) and earth-fixed (inertial) coordinate systems for the projectile trajectory analysis with the corresponding orientation definitions (Euler angles).

Two main coordinate systems are used for the computational approach of the atmospheric flight motion. The one is a plane fixed (inertial frame, IF) at the ground surface, which it's center O1 lies on ground surface, as depicted in Fig. 3. The other is a no-roll rotating coordinate system that is attached to, and moving with, the projectile's center of mass O2 (no-roll-frame, NRF, φ = 0) with X_{NRF} axis along the projectile's axis of rotational symmetry positive from tail to nose. Y_{NRF} axis is perpendicular to X_{NRF} lying in the horizontally plane. Z_{NRF} axis oriented so as to complete a right-hand orthogonal system.
Newton's laws of the motion state that the rate of change of linear momentum must equal the sum of all the externally applied forces and the rate of change of angular momentum must equal the sum of the externally applied moments, as shown respectively in the following forms:

$$m\frac{d\vec{V}}{dt} = \vec{F}_{tot} \tag{1}$$

$$\frac{d\vec{H}}{dt} = \vec{M}_{tot} \tag{2}$$

The twelve state variables x, y, z, φ, θ, ψ, $\tilde{u}$, $\tilde{v}$, $\tilde{w}$, $\tilde{p}$, $\tilde{q}$ and $\tilde{r}$ are necessary to describe position, flight direction and velocity at every point of the projectile's atmospheric trajectory. Introducing the components of the acting forces and moments expressed in the no-roll-frame, the following 6-DOF equations of motion, with respect to time t, are derived:

$$\dot{x}_{if} = \cos\theta\cos\psi\,\tilde{u}_{NRF} - \sin\psi\cdot\tilde{v}_{NRF} + \sin\theta\cos\psi\cdot\tilde{w}_{NRF} \tag{3}$$

$$\dot{y}_{if} = \cos\theta\sin\psi\,\tilde{u}_{NRF} + \cos\psi\cdot\tilde{v}_{NRF} + \sin\theta\sin\psi\cdot\tilde{w}_{NRF} \tag{4}$$

$$\dot{z}_{if} = -\sin\theta\,\tilde{u}_{NRF} + \cos\theta\cdot\tilde{w}_{NRF} \tag{5}$$

for the position of projectile's center of mass and

$$\dot{\varphi} = \tilde{p}_{NRF} + t_\theta \cdot \tilde{r}_{NRF} \quad (6)$$

$$\dot{\theta} = \tilde{q}_{NRF} \quad (7)$$

$$\dot{\psi} = \frac{1}{\cos\theta} \cdot \tilde{r}_{NRF} \quad (8)$$

and for the orientation of the flight body with the classical Euler angles φ, θ, ψ. From the two laws of Newton's motion the following equations are derived, respectively:

$$\dot{\tilde{u}}_{NRF} = \frac{1}{m}\tilde{F}_{x_{total}} + \tilde{r}_{NRF} \cdot \tilde{v}_{NRF} - \tilde{q}_{NRF} \cdot \tilde{w}_{NRF} \quad (9)$$

$$\dot{\tilde{v}}_{NRF} = \frac{1}{m}\tilde{F}_{y_{total}} - \tilde{r}_{NRF} \cdot \tilde{u}_{NRF} - \tilde{r}_{NRF} \cdot t_\theta \cdot \tilde{w}_{NRF} \quad (10)$$

$$\dot{\tilde{w}}_{NRF} = \frac{1}{m}\tilde{F}_{z_{total}} + \tilde{q}_{NRF} \cdot \tilde{u}_{NRF} + \tilde{r}_{NRF} \cdot t_\theta \cdot \tilde{v}_{NRF} \quad (11)$$

$$\begin{pmatrix} \dot{\tilde{p}}_{NRF} \\ \dot{\tilde{q}}_{NRF} \\ \dot{\tilde{r}}_{NRF} \end{pmatrix} = I^{-1} \cdot \left(\begin{pmatrix} \tilde{L}_{TOTAL} \\ \tilde{M}_{TOTAL} \\ \tilde{N}_{TOTAL} \end{pmatrix} - X_1 \cdot X_2 \right) \quad (12)$$

where

$$X_1 = \begin{pmatrix} 0 & -\tilde{r}_{NRF} & \tilde{q}_{NRF} \\ \tilde{r}_{NRF} & 0 & \tilde{r}_{NRF} \cdot t_\theta \\ -\tilde{q}_{NRF} & -\tilde{r}_{NRF} \cdot t_\theta & 0 \end{pmatrix}$$

$$X_2 = \begin{pmatrix} I_{XX} & I_{XY} & I_{XZ} \\ I_{YX} & I_{YY} & I_{YZ} \\ I_{ZX} & I_{ZY} & I_{ZZ} \end{pmatrix} \cdot \begin{pmatrix} \tilde{p}_{NRF} \\ \tilde{q}_{NRF} \\ \tilde{r}_{NRF} \end{pmatrix}$$

The total force acting on the projectile in Eq. (12) comprises the weight W_f, the aerodynamic force A_f and Magnus force M_f:

$$\tilde{F}_{x_{TOTAL}} = \tilde{X}_{W_f} + \tilde{X}_{A_f} + \tilde{X}_{M_f} \quad (13)$$

$$\tilde{F}_{y_{TOTAL}} = \tilde{Y}_{W_f} + \tilde{Y}_{A_f} + \tilde{Y}_{M_f} \quad (14)$$

$$\tilde{F}_{z_{TOTAL}} = \tilde{Z}_{W_f} + \tilde{Z}_{A_f} + \tilde{Z}_{M_f} \quad (15)$$

The total moment acting on the projectile in Eq. (13), (14) and (15) comprises the moment due to the standard aerodynamic force A_m, due to Magnus aerodynamic force M_m and the unsteady aerodynamic moment UA_m:

$$\tilde{L}_{TOTAL} = \tilde{L}_{A_m} + \tilde{L}_{M_m} + \tilde{L}_{UA_m}$$

$$\tilde{M}_{TOTAL} = \tilde{M}_{A_m} + \tilde{M}_{M_m} + \tilde{M}_{UA_m}$$

$$\tilde{N}_{TOTAL} = \tilde{N}_{A_m} + \tilde{N}_{M_m} + \tilde{N}_{UA_m}$$

All aerodynamic coefficients are based on Mach number and the aerodynamic angles of attack and sideslip:

$$\alpha = \tan^{-1}\left(\frac{\tilde{w}_{NRF}}{\tilde{u}_{NRF}} \right) \quad (16)$$

$$\beta = \tan^{-1}\left(\frac{\tilde{v}_{NRF}}{\tilde{u}_{NRF}} \right) \quad (17)$$

The total aerodynamic velocity given in equation:

$$V = \sqrt{\tilde{u}_{NRF}^{\,2} + \tilde{v}_{NRF}^{\,2} + \tilde{w}_{NRF}^{\,2}} \quad (18)$$

The weight force in no-roll system is:

$$\begin{Bmatrix} \tilde{X}w_f \\ \tilde{Y}w_f \\ \tilde{Z}w_f \end{Bmatrix} = mg \begin{Bmatrix} -\sin\theta \\ 0 \\ \cos\theta \end{Bmatrix} \quad (19)$$

The aerodynamic force, which acts on the projectile at aerodynamic center of pressure, is:

$$\begin{pmatrix} \tilde{X}_{Af} \\ \tilde{Y}_{Af} \\ \tilde{Z}_{Af} \end{pmatrix} = -\frac{1}{2}\rho V^2 S_{ref} \begin{pmatrix} C_{D0} + C_{D\delta^2}\delta^2 \\ (C_D + C_{La})\dfrac{\tilde{v}_{NRF}}{V} \\ (C_D + C_{La})\dfrac{\tilde{w}_{NRF}}{V} \end{pmatrix} \quad (20)$$

The Magnus, which acts on projectile at the Magnus force center of pressure, is:

$$\begin{pmatrix} \tilde{X}_{M_f} \\ \tilde{Y}_{M_f} \\ \tilde{Z}_{M_f} \end{pmatrix} = \frac{1}{2}\rho V^2 S_{ref} \begin{pmatrix} 0 \\ \dfrac{\tilde{p}_{NRF} DC_{NPA} \tilde{w}_{NRF}}{2V^2} \\ \dfrac{-\tilde{p}_{NRF} DC_{NPA} \tilde{v}_{NRF}}{2V^2} \end{pmatrix}$$

The moment due to aerodynamic force is:

$$\begin{pmatrix} \tilde{L}_{A_m} \\ \tilde{M}_{A_m} \\ \tilde{N}_{A_m} \end{pmatrix} = \begin{bmatrix} 0 & 0 & 0 \\ 0 & 0 & -R_{\oplus MAC} \\ 0 & R_{\oplus MAC} & 0 \end{bmatrix} \begin{bmatrix} \tilde{X}_{Af} \\ \tilde{Y}_{Af} \\ \tilde{Z}_{Af} \end{bmatrix}$$

The moment due to Magnus force is:

$$\begin{pmatrix} \tilde{L}_{M_m} \\ \tilde{M}_{M_m} \\ \tilde{N}_{M_m} \end{pmatrix} = \begin{bmatrix} 0 & 0 & 0 \\ 0 & 0 & -R_{\oplus MAX} \\ 0 & R_{\oplus MAX} & 0 \end{bmatrix} \begin{bmatrix} \tilde{X}_{Mf} \\ \tilde{Y}_{Mf} \\ \tilde{Z}_{Mf} \end{bmatrix}$$

In addition, for the unsteady moment UA_m is:

$$\begin{pmatrix} \tilde{L}_{UA_m} \\ \tilde{M}_{UA_m} \\ \tilde{N}_{UA_m} \end{pmatrix} = \frac{1}{2}\rho V^2 D S_{ref} \begin{pmatrix} \dfrac{\tilde{p}_{NRF} \cdot DC_{LP}}{2V} \\ \dfrac{\tilde{q}_{NRF} \cdot DC_{MQ}}{2V} + \dfrac{C_{MA}}{V} \\ \dfrac{\tilde{r}_{NRF} \cdot DC_{MQ}}{2V} - \dfrac{C_{MA}}{V} \end{pmatrix}$$

If the independent variable is changed from time t to dimensionless arc length *l* measured in calibers of travel

$$l = \frac{1}{D}s = \frac{1}{D}\int_0^t V_T dt \tag{21}$$

The following relationship between the arc length and time derivatives exist:

$$\xi' = \frac{D}{V_T}\dot{\xi} \tag{22}$$

Application of the previous Eq. (22) yield the following 6-DOF atmospheric equations of motion expressed in the no-roll frame

$$x'_{if} = \frac{D}{V_T}\cos\psi\cos\theta \cdot \tilde{u}_{NRF} - \frac{D}{V_T}\sin\psi \cdot \tilde{v}_{NRF} + \frac{D}{V_T}\cos\psi\sin\theta \cdot \tilde{w}_{NRF} \tag{23}$$

$$y'_{if} = \frac{D}{V_T}\cos\theta\sin\psi \cdot \tilde{u}_{NRF} + \frac{D}{V_T}\cos\psi \cdot \tilde{v}_{NRF} + \frac{D}{V_T}\sin\psi\sin\theta \cdot \tilde{w}_{NRF} \tag{24}$$

$$z'_{if} = -\frac{D}{V_T}\sin\theta\tilde{u}_{NRF} + \frac{D}{V_T}\cos\theta\tilde{w}_{NRF} \tag{25}$$

$$\phi' = \frac{D}{V_T}\tilde{p}_{NRF} + \frac{D}{V_T}\tan\theta\,\tilde{r}_{NRF} \tag{26}$$

$$\theta' = \frac{D}{V_T}\tilde{q}_{NRF} \tag{27}$$

$$\psi' = \frac{D}{V_T\cos\theta}\tilde{r}_{NRF} \tag{28}$$

$$\tilde{u}'_{NRF} = -\frac{D}{V_T}g\sin\theta - L_1 V_T C_D + \tilde{v}_{NRF}\frac{D}{V_T}\tilde{r}_{NRF} - \tilde{q}_{NRF}\frac{D}{V_T}\tilde{w}_{NRF} \tag{29}$$

$$\tilde{v}'_{NRF} = -L_1\left(C_{La} + C_D\right)\tilde{v}_{NRF} - \frac{D}{V_T}\cdot\tilde{r}_{NRF}\cdot\tilde{w}_{NRF}\tan\theta - \frac{D}{V_T}\cdot\tilde{u}_{NRF}\cdot\tilde{r}_{NRF} \tag{30}$$

$$\tilde{w}'_{NRF} = \frac{D}{V_T}g\cos\theta - L_1 C_{L_a}\tilde{w}_{NRF} - L_1 C_D\tilde{w}_{NRF} + \tilde{u}_{NRF}\frac{D}{V_T}\tilde{q}_{NRF} + \tan\theta\frac{D}{V_T}\tilde{r}_{NRF}\tilde{v}_{NRF} \tag{31}$$

$$\tilde{p}'_{NRF} = D^5\frac{\pi}{16I_{XX}}\tilde{p}_{NRF}\rho C_{LP} \tag{32}$$

$$\begin{aligned}\tilde{q}'_{NRF} &= 2L_2 C_{La}\cdot\tilde{w}_{NRF} L_{CGCP} + \\ &+ 2L_2 C_D\cdot\tilde{w}_{NRF} L_{CGCP} + \\ &+ D\frac{L_2}{V_T} C_{MPA}\,\tilde{p}_{NRF}\,\tilde{v}_{NRF} L_{CGCM} + \\ &+ D^2 L_2 C_{MQ}\,\tilde{q}_{NRF} + 2D\,L_2 C_{MA} - \\ &- \frac{D}{V_T}\tilde{r}_{NRF}\frac{I_{XX}}{I_{YY}}\tilde{p}_{NRF} - \frac{D}{V_T}\tilde{r}^2_{NRF}\tan\theta\end{aligned} \quad (33)$$

$$\begin{aligned}\tilde{r}'_{NRF} &= -2L_2\cdot C_{La}\cdot\tilde{v}_{NRF}\cdot L_{CGCP} - \\ &- 2L_2\cdot C_D\cdot\tilde{v}_{NRF}\cdot L_{CGCP} + \\ &+ D\frac{L_2}{V_T}\tilde{p}_{NRF}\cdot C_{MPA}\cdot\tilde{w}_{NRF} L_{CGCM} + \\ &+ D^2 L_2 C_{MQ}\cdot\tilde{r}_{NRF} - 2DL_2 C_{MA} + \\ &+ \frac{D}{V_T}\tilde{p}_{NRF}\cdot\tilde{q}_{NRF}\frac{I_{XX}}{I_{YY}} + \\ &+ \frac{D}{V_T}\tilde{q}_{NRF}\cdot\tilde{r}_{NRF}\tan\theta\end{aligned} \quad (34)$$

The projectile dynamics trajectory model consists of twelve highly first order ordinary differential equations (23)-(34), which are solved simultaneously by resorting to numerical integration using a 4th order Runge-Kutta method. In these equations, the following sets of simplifications are employed: velocity $\tilde{u}$ replaced by the total velocity V because the side velocities $\tilde{v}$ and $\tilde{w}$ are small. The aerodynamic angles of attack α and sideslip β are small for the main part of the atmospheric trajectory $\alpha \approx \tilde{w}/V, \beta \approx \tilde{v}/V$, the projectile is geometrically symmetrical $I_{XY} = I_{YZ} = I_{XZ} = 0$, $I_{YY} = I_{ZZ}$ and aerodynamically symmetric. With the afore-mentioned assumptions, the expressions of the distance from the center of mass to the standard aerodynamic and Magnus centers of pressure are simplified.

4 Aerodynamic Model

For the projectiles trajectory analysis the constant flight dynamic model is based on appropriate constant mean values of the experimental average aerodynamic coefficients variations taking from official tabulated database [15], as shown in Table 2.

Aerodynamic Coefficients		**120 mm**	**40 mm**
Drag	C_D	0.14	0.279
Lift	C_{La}	10.76	2.329
Pitch Damping	C_{MQ}	-22.3	-1.8
Overturning Moment	C_{MA}	-15.76	0

Table 2. Aerodynamic parameters of atmospheric flight dynamic model.

5 Atmospheric Model

Atmospheric properties of air, like density ρ, are being calculated based on a standard atmosphere from the International Civil Aviation Organization (ICAO).

6 Initial Spin Rate Estimation

In order to have a statically stable flight for spin-stabilized projectile trajectory motion, the initial spin rate $\tilde{p}_o$ prediction at the gun muzzle in the firing site us important. According to McCoy definitions, the following form is used:

$$\tilde{p}_o = 2\pi V_o / \eta D \quad (rad/s) \quad (35)$$

where V_o is the initial firing velocity (m/s), η the rifling twist rate at the gun muzzle (calibers per turn), and D the reference diameter of the projectile type (m). Typical values of rifling twist η are 1/30 calibers per turn for 40mm projectile. The 120 mm mortar projectile has uncanted fins, and do not roll or spin at any point along the trajectory.

7 Computational Simulation

The flight dynamic models of 40 mm grenade and 120 mm HE mortar projectile types involves the solution of the set of the twelve first order ordinary differentials, Eqs (23-34), which are solved simultaneously by resorting to numerical integration using a 4th order Runge-Kutta method, and regard to the 6-D nominal atmospheric projectile flight.

The results give the computational simulation of the 6-D non-thrusting and non-constrained flight trajectory path for some specific spin and fin-projectiles types. Initial flight conditions for both dynamic flight simulation models with constant and variable aerodynamic coefficients are illustrated in Table 3 for the examined test cases.

Initial flight data	**40mm grenade, M781**	**120mm mortar projectile**
x, m	0.0	0.0
y, m	0.0	0.0
z, m	0.0	0.0
φ, deg	0.0	0.0
θ, deg	14.7^o , 30^o and 40^o	45^o , 65^o and 85^o

ψ, deg	2.0	3.0
u, m/s	74.7	318.0
v, m/s	0.0	0.0
w, m/s	0.0	0.0
p, rad/s	376.0	0.0
q, rad/s	0.0	1.795
r, rad/s	0.0	0.0

Table 3. Initial flight parameters of the projectile examined test cases

8 Results and Discussion

The flight path trajectory motion with constant aerodynamic coefficients of the 40 mm grenade with initial firing velocity of 74.7 m/sec, initial yaw angle 2 degrees, at 14.7°, 30° and 40°, respectively, are indicated in Fig. 4. The calculated impact points of the above no-wind trajectories with the proposed constant aerodynamic coefficients [12] compared with technical recognized data.

The mortar projectile of 120 mm diameter is also examined for its atmospheric constant flight trajectories predictions in at pitch angles of 45°, 65°, 85°, with initial firing velocity of 318 m/s, initial yaw angle 3° and pitch rate 1.795 rad/s. The impact points of the above trajectories are compared with an accurately flight path prediction with McCoy's trajectory data [15] as presented in Fig. 5.

From the results of the presented applied method, at 14.7° pitch angle, the maximum range is 235 m and the maximum height is almost 16.7 m, at 30°, the proposed trajectory simulation gives 367 m and 60.5 m, and at 40°gives 398 m and 97 m respectively as shown in Fig. 4.

At 45°, the 120 mm mortar projectile, fired at no wind conditions, gives a range to impact at 7,000 m with a maximum height at almost 2050 m. At 65°, the predicted level-ground range is approximately 5,320 m and the height is 3,280 m and at 85° gives 1,235m and 3,950m respectively. For the same initial pitch angles, the 120 mm mortar projectile of McCoy's data has longer range to impact points.

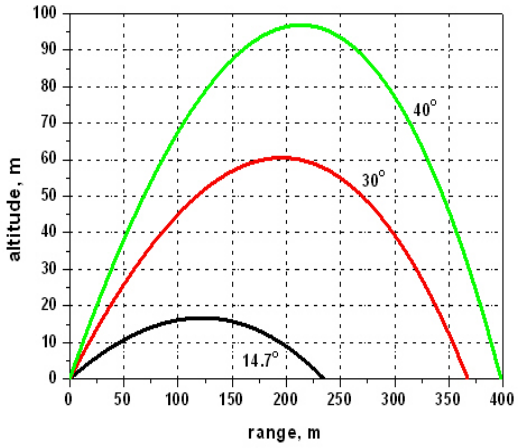

Fig. 4. Impact points and flight path trajectories for 40 mm projectile

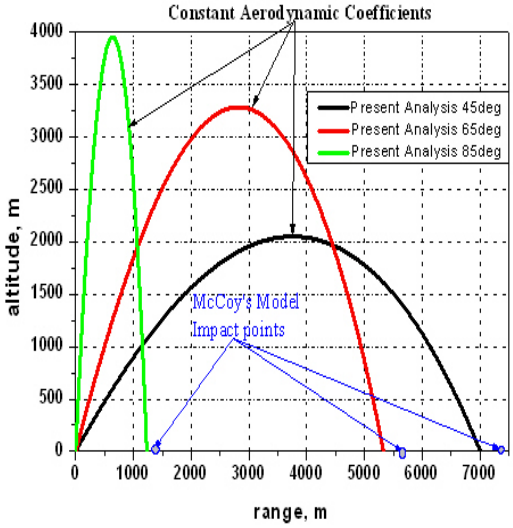

Fig. 5. Impact points and flight path trajectories with constant aerodynamic coefficients for 120 mm at quadrant elevation angles of 45°, 65° and 85° compared with McCoy's model data

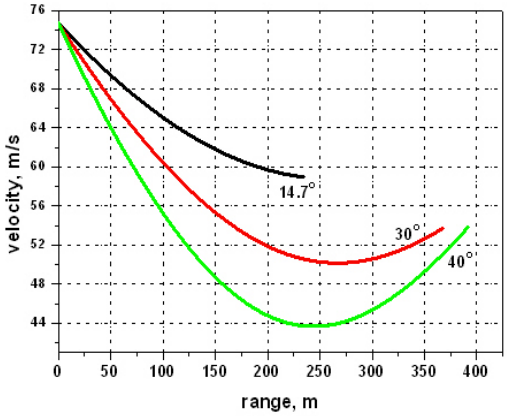

Fig. 6. Velocity trajectories at elevation angles of 14.7, 30 and 40 degrees, for 40 mm projectile

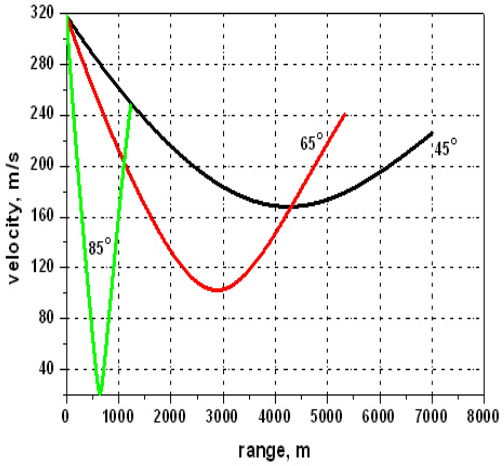

Fig. 7. Velocity variations of 120 mm, at pitch angles of 45, 65 and 85 degrees

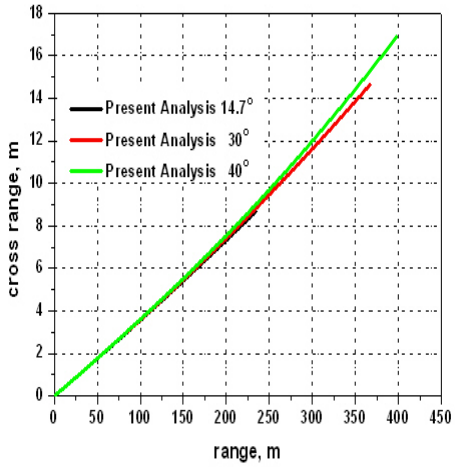

Fig. 8. Cross range versus range for 40 mm projectile

Comparative computed trajectories of the 40 mm projectile at pitch angles of 14.7°, 30° and 40° are indicated in Fig. 8. From the computational results of the applied method at 14, 7°, the velocity decreases to the value of 59 m/sec at the impact point, at 30 degrees decreases to 50 and then grows to the value of almost 53 m/sec, and at pitch angle of 40 degrees, the velocity gives the value of 43 and then grows to the value of 53 m/sec.

Furthermore, the computational results for 120 mm projectile at elevation angles of 45°, 65° and 85° are illustrated in Fig. 7. At pitch angle of 45 degrees, the velocity decreases to the value of almost 170 and then grows to the value of 235 m/sec. At pitch angle of 65 degrees, the velocity decreases to the value of almost 100 and then grows to the value of 240 m/sec. Moreover, at pitch angle of 85 degrees the velocity decreases to value of 20 and then grows to the value of 250 m/sec.

Figures 8 and 9 show the deflection of the flight trajectory at sea level with no-wind for the 40 mm projectile at pitch angles of 14.7^o , 30^o , 45^o and for 120 mm projectile at elevation angles 45^o , 65^o , 85^o respectively. The present analysis trajectory of the 40 mm projectile with initial firing velocity of 74.7 m/sec and positive yaw angle 2 degrees at pitch angles of 14.7^o, 30^o , 45^o gives positive (right) deflection at about 8.7 m, 14.5 m, 17 m respectively. Moreover, the mortar projectile of 120 mm diameter with initial firing velocity of 318 m/s, initial yaw angle 3 degrees and pitch rate 1.795 rad/s, gives always positive values of cross range 380 m, 290 m and 65 m at various low and high pitch angles, respectively.

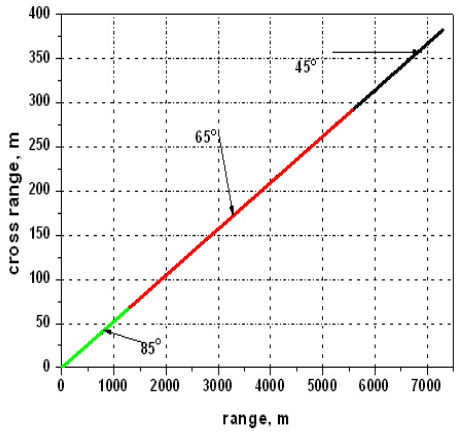

Fig. 9. Cross range computational predictions of 120 mm mortar projectile at elevation angles of 45^o, 65^o and 85^o

9 Conclusion

The complicated six degrees of freedom (6-DOF) simulation flight dynamics model is applied for the accurate prediction of short and long-range trajectories of high and low spin and fin-stabilized projectiles. It takes into consideration the Mach number and the total angle of attack variation effects by means of the constant aerodynamic coefficients. The computational results of the proposed synthesized analysis are in good agreement compared with other technical data and recognized exterior atmospheric projectile flight computational models.

References

[1] Amoruso, M. J., *Euler Angles and Quaternions in Six Degree of Freedom Simulations of Projectiles*, Technical Note, March 1996.

[2] Bundy, M., T*he regional nature of aerodynamic jump*, Ballistic Research Laboratories Report No.1872, 1999.

[3] Burchett, B., Peterson, A., and Costello, M., Prediction of swerving motion of a dual-spin projectile with lateral pulse jets in atmospheric flight, *Mathematical and Computer Modeling*, Vol. 35, No. 1-2, 2002, pp. 1-14.

[4] Carlucci, E. D., Jacobson, S, S., *Ballistics: Theory and Design of Guns and Ammunition*, CRC Press, Taylor and Francis Group, 2008.

[5] Cooper, G., Influence of yaw cards on the growth of spin stabilized projectiles, *Journal of aircraft*, Vol.38, No. 2, 2001, pp.266-270.

[6] Cooper, G., Extending the Jump Analysis for Aerodynamic Asymmetry, *Army Research Laboratory*, ARL-TR-3265, 2004.

[7] Cooper, G., Projectile Aerodynamic Jump Due to Lateral Impulsives , *Army Research Laboratory*, ARL-TR-3087, 2003.

[8] Costello, M. F., Anderson, D. P., *Effect of Internal Mass Unbalance on the Terminal Accuracy and Stability of a Projectile*, *AIAA Paper* 96-3447, 1996.

[9] Costello, M., and Peterson, A., Linear theory of a dual-spin projectile in atmospheric flight, *Journal of Guidance, Control, and Dynamics*, Vol.23, No5, 2000, pp.789-797.

[10] Etkin, B., *Dynamics of Atmospheric Flight*, John Wiley and Sons, New York, 1972.

[11] Fowler, R., Gallop, E., Lock, C., and Richmond, H., The aerodynamics of spinning shell, *Philosophical Transactions of the Royal Society of London, Series A: Mathematical and Physical Sciences*, Vol.221, 1920.

[12]Gkritzapis, D., N., Panagiotopoulos, E. E., Margaris, D. P., Papanikas, D. G., Atmospheric Flight Dynamic Simulation Modelling of Spin-Stabilized Projectiles, *Proceedings of the 2nd International Conference on Experiments / Process / System Modelling / Simulation / Optimization*, 2nd IC-EpsMsO, 4-7 July 2007, Athens, Greece.

[13]Guidos, B., and Cooper, G., Closed form solution of finned projectile motion subjected to a simple in-flight lateral impulse, *AIAA Paper* 2000-0767, 2000.

[14] Hainz, L. C., Costello, M., Modified Projectile Linear Theory for Rapid Trajectory Prediction, *Journal of Guidance, Control and Dynamics*, Vol. 28, No. 5, Sept-Oct 2005.

[15]McCoy, R. L.: *Modern Exterior Ballistics*, Schiffer, Attlen, PA, 1999.

[16]Murphy, C. H., Circular Pitching and Yawing Motion of Nose Cone Configurations, *Planetary and Space Science*, Vol. 4, 1961, pp. 328-336.

[17] Murphy, C., Instability of Controlled Projectiles in Ascending or Descending Flight, *Journal of Guidance, Control, and Dynamics*, Vol. 4, No. 1, 1981.

[18] Sterne, T. H., "*On Jump due to bore clearance*," Ballistic Research Laboratories Report No.491, 1944.

[19] Rasmussen, M. L., Kirk, D. B.: "*On the Pitching and Yawing Motion of a Spinning Symmetric Missile Governed by an Arbitrary Nonlinear Restoring Moment*", NASA TN D-2135, 1964.

A List of Symbols

a_t = total angle of attack, $a_t = \sqrt{a^2 + \beta^2}$, deg

C_D = drag force aerodynamic coefficient
C_{La} = lift force aerodynamic coefficient
C_{LP} = roll damping moment aerodynamic coefficient
C_{MQ}= pitch damping moment aerodynamic coefficient
C_{MA}= overturning moment aerodynamic coefficient
C_{MPA} = Magnus moment aerodynamic coefficient
D = projectile reference diameter, m
$\vec{F}$ = vector sum of all aerodynamic forces
g = sea-level acceleration gravity, 9.80665 m/s^2
$\vec{H}$ = total vector angular momentum of the projectile
I_{XX} = projectile axial moment of inertia, kg·m^2
I_{YY} = projectile transverse moment of inertia about y-axis through the center of mass, kg·m^2
I_{XX}, I_{YY}, I_{ZZ} = diagonal components of the inertia matrix
L_{CGCM} = distance from the center of mass (CG) to the Magnus center of pressure (CM) along the station line, m
L_{CGCP} = distance from the center of mass (CG) to the aerodynamic center of pressure (CP) along the station line, m
l = dimensionless arc length
$\vec{M}$ = vector sum of all aerodynamic moments
m = projectile m ass, kg
$\tilde{p}, \tilde{q}, \tilde{r}$ = projectile roll, pitch and yaw rates in the moving frame (NRF), respectively, rad/s
S_{ref} = projectile reference area ($\frac{\pi D^2}{4}$), m^2
t = time
$\tilde{u}, \tilde{v}, \tilde{w}$ = projectile velocity components expressed in the no-roll-frame (NRF), m/s
V = total aerodynamic velocity, m/s
V_T = total velocity, m/s
V_o = total muzzle velocity, m/s
x, y, z = projectile position coordinates in the inertial frame (if), m

GREEK SYMBOLS

α, β = aerodynamic angles of attack and sideslip, deg

δ = $\sin a_t$

η = rifling twist rate of the machine gun, calibers/turn

ρ = density of air, kg/m^3

φ, θ, ψ = projectile roll, pitch and yaw angles, respectively, deg

SUBSCRIPTS

o = initial values at the firing site